Frontiers in Bioscience Landmark

Front. Biosci. (Landmark Ed) **2026**; 31(8): 54257
https://doi.org/10.31083/FBL54257

Original Research

Calcium Channel Blockers Modulate Calcium Homeostasis and Signaling Gene Expression in *Sophora tonkinensis*

Ying Liang[1,2], Shuangshuang Qin[1,2], Guili Wei[1,2], Yuan Huang[1,2], Hong He[1,2], Fan Wei[1,2,*]

[1]Guangxi Key Laboratory of Medicinal Resources Protection and Genetic Improvement, National Center for Traditional Chinese Medicine (TCM) Inheritance and Innovation, Guangxi Botanical Garden of Medicinal Plants, 530023 Nanning, Guangxi, China
[2]National Engineering Research Center for Southwest Endangered Medicinal Materials Resources Development, Guangxi Botanical Garden of Medicinal Plants, 530023 Nanning, Guangxi, China
*Correspondence: fanwei_gx@163.com (Fan Wei)
Academic Editor: Jen-Tsung Chen
Submitted: 26 May 2026 Revised: 9 July 2026 Accepted: 21 July 2026 Published: 11 August 2026

Abstract

Background: Calcium signaling plays a critical role in plant growth, development, and stress adaptation. However, the tissue-specific mechanisms governing calcium homeostasis in medicinal plants adapted to high-calcium karst environments remain poorly understood. This study investigated the functional divergence and potential molecular basis of calcium homeostasis in leaves and root tips of *Sophora tonkinensis* under pharmacological perturbation. **Methods:** Treatments included lanthanum chloride ($LaCl_3$) (a plasma membrane Ca^{2+} channel blocker), sodium orthovanadate (Na_3VO_4) (a Ca^{2+}-ATPase inhibitor), and ethylene glycol-bis(β-aminoethyl ether)-N,N,N′,N′-tetraacetic acid (EGTA) (an extracellular Ca^{2+} chelator). Subcellular calcium distribution and expression of 14 calcium signaling-related genes were analyzed at 20, 40, and 60 days post-treatment using potassium pyroantimonate precipitation in conjunction with transmission electron microscopy and quantitative real-time PCR. **Results:** $LaCl_3$ treatment initially induced intracellular calcium accumulation, followed by the engagement of alternative efflux pathways in leaves and increased extracellular deposition in root tips. Na_3VO_4 treatment exacerbated intracellular calcium overload, resulting in sustained calcium toxicity in leaves, whereas root tips exhibited coordinated calcium redistribution. EGTA treatment dampened overall calcium signaling. However, root tips maintained functionality by mobilizing internal calcium stores. Gene expression analysis revealed a significant upregulation of *Sophora tonkinensis* calmodulin-like protein 9 (*StCML9*) in roots (up to 11.7-fold relative to the control), with expression closely synchronized with Ca^{2+} fluctuations, suggesting a potential role for *StCML9* in calcium sensing and adaptive responses. In contrast, *Sophora tonkinensis* calcium-dependent protein kinases (*StCDPKs*) were generally suppressed in leaves. **Conclusions:** These findings suggest that *S. tonkinensis* may employ organ-specific calcium distribution and transcriptional reprogramming to maintain calcium homeostasis under signaling perturbation. This study provides correlative evidence that contributes to mechanistic insights into the species' adaptation to high-calcium karst environments and offers candidate genes for future functional validation.

Keywords: *Sophora tonkinensis*; calcium channel blockers; cellular structures; calcium signaling; organ specificity

1. Introduction

Calcium ions (Ca^{2+}) serve as highly conserved second messengers in eukaryotes, playing critical roles in plant growth, development, and responses to environmental stresses [1,2]. Plant cells regulate dynamic fluctuations in cytosolic free Ca^{2+} concentrations through the coordinated action of the cell wall, plasma membrane Ca^{2+} channels, and intracellular Ca^{2+} stores, such as the vacuole and endoplasmic reticulum. These fluctuations generate 'Ca^{2+} signatures' that are decoded to activate downstream responses [3,4]. These processes are integral to photomorphogenesis [5], tropic growth [6], and adaptive responses to biotic and abiotic stresses, including drought, salinity, extreme temperatures, and pathogen infection [7,8,9]. Consequently, Ca^{2+} signaling is central to nearly all aspects of plant life [10]. In many studies, pharmacological blockers have been used to demonstrate the key functions of Ca^{2+} signaling in the control of root growth [11,12], antioxidant enzyme activities [13,14], secondary metabolite accumulation [15,16] and disease resistance [17,18], such as lanthanum chloride ($LaCl_3$) (a plasma membrane Ca^{2+} channel blocker), ethylene glycol-bis(β-aminoethyl ether)-N,N,N′,N′-tetraacetic acid (EGTA) (an extracellular Ca^{2+} chelator) and sodium orthovanadate (Na_3VO_4) (a Ca^{2+}-ATPase inhibitor).

Sophora tonkinensis Gagnep., a valuable medicinal plant native to the calcium-rich karst regions of China, exhibits significant environmental adaptation through calcium signaling [19]. A prior study has indicated that exogenous calcium treatment influences the growth, physiological traits, and medicinal compound accumulation of *S. tonkinensis* [20], underscoring a crucial role for Ca^{2+} signaling in its environmental adaptation and secondary metabolism. However, the mechanisms governing calcium homeostasis

in *S. tonkinensis* remain inadequately explored. Specifically, the dynamic responses of distinct subcellular Ca^{2+} pools (such as those in the plasma membrane, vacuole, and cell wall) to external perturbations have not been systematically investigated. In addition, the coordination of key components in the Ca^{2+} signaling pathway (including Ca^{2+}-ATPase, Cation/H^+ Exchanger (CAX), phospholipase C (PLC), calcium-dependent protein kinase (CDPK), and calmodulin-like protein (CML)) across different tissues like roots and leaves remains unclear.

A pharmacological approach was used to examine the effect of different Ca^{2+} signaling pathways on *S. tonkinensis* plantlets using three different inhibitors: $LaCl_3$, Na_3VO_4, and EGTA, which have different modes of action. Subcellular calcium distribution was detected by precipitation of potassium pyroantimonate, and expression levels of calcium signaling-related genes were quantified by quantitative real-time PCR (qRT-PCR). This study aims to investigate the tissue-specific regulatory mechanisms involved in the control of the intracellular calcium homeostasis of *S. tonkinensis* under these treatments by comparing the temporal responses of leaves and roots. These findings may offer a theoretical framework to explain the role of calcium signaling in the growth, development, and secondary metabolism of medicinal plants.

2. Materials and Methods

2.1 Plant Materials and Treatment With Calcium Channel Blockers

Tissue-cultured plantlets of the medicinal plant *S. tonkinensis* were utilized as experimental materials. The plantlets were maintained under controlled conditions of 25 ± 1 °C, 16 h light/8 h dark photoperiod with a light intensity of 120 $\mu mol \cdot m^{-2} \cdot s^{-1}$ provided by cool-white fluorescent lamps (Shenzhen Vanq Technology Co., Ltd., Shenzhen, Guangdong, China).

The plant material was sourced from the Guangxi Botanical Garden of Medicinal Plants, Nanning, Guangxi, China (22°51’12” N, 108°22’38” E). The plant material was identified by Associate Professor Fan Wei (Guangxi Botanical Garden of Medicinal Plants). Voucher specimens (accession No. YYZW20240189) were deposited in the Germplasm Repository of the Guangxi Botanical Garden of Medicinal Plants.

To perturb specific pathways of intracellular calcium signaling, various calcium channel blockers were introduced into the culture medium. All blockers were dissolved in sterile distilled water as stock solutions, filter-sterilized (0.22 μm pore size), and added to the culture medium after autoclaving and cooling to approximately 50–55 °C to prevent thermal degradation. The final concentrations in the culture medium were as follows: R1: 50 μM $LaCl_3$ (449830, Sigma-Aldrich, St. Louis, MO, USA), R2: 50 μM Na_3VO_4 (S6508, Sigma-Aldrich), R3: 0.5 mM EGTA (E3889, Sigma-Aldrich). The control group (R0) received an equivalent volume of sterile distilled water.

The culture medium for all groups comprised 1/2 MS medium (Murashige and Skoog, 1962 [21]; MSP01, PhytoTechnology Laboratories, Shawnee Mission, KS, USA) supplemented with 1.5 mg/L naphthaleneacetic acid (NAA) (PHA0034, Duly Biotech, Nanjing, Jiangsu, China) and 0.3 mg/L indole-3-acetic acid (IAA) (PHA0031, Duly Biotech), with a pH adjusted to 5.8. Root and leaf tissues were harvested from each group at 20, 40, and 60 days after inoculation, with three biological replicates per treatment. Total RNA extraction was performed on the tissue samples, which were immediately frozen in liquid nitrogen upon collection and stored at –80 °C.

The extended treatment durations (20, 40, and 60 days) were selected to investigate long-term adaptive responses of calcium homeostasis, as calcium signaling events under chronic pharmacological perturbation require extended periods for observable phenotypic and transcriptional changes.

2.2 Sample Preparation for Transmission Electron Microscopy and Pyroantimonate Precipitation

Following treatment with the calcium channel blockers, leaf and root tip tissues were rinsed with ice-cold phosphate-buffered saline (PBS). Small pieces approximately 1 mm^3 in size were then excised and immersed in ice-cold fixative solution (0.1 M phosphate buffer (R29808-500 mL, Shanghai Yuanye Bio-Technology, Shanghai, China)) containing 2.5% glutaraldehyde (16220, Electron Microscopy Sciences, Hatfield, PA, USA) and 2% potassium pyroantimonate (P815763, Shanghai Macklin Biochemical, Shanghai, China, pH 7.4) for fixation at 4 °C for 2 to 4 hours. After fixation, the samples were rinsed three times with 0.1 M phosphate washing buffer containing 2% potassium pyroantimonate, with each wash lasting 15 minutes. The samples were then transferred to a solution of 1% osmium tetroxide (18456, Ted Pella Inc., Redding, CA, USA) containing 2% potassium pyroantimonate and post-fixed overnight at 4 °C.

The samples were subsequently dehydrated through a graded ethanol series (30%, 50%, 70%, 80%, 95%, 100% I, 100% II) and propylene oxide (80059118, Sinopharm Chemical Reagent, Shanghai, China) before infiltration and embedding in Epon-812 epoxy resin (18010, TED PELLA, Redding, CA, USA). The embedded samples were polymerized at 60 °C for 48 hours. Ultrathin sections (70 nm) were prepared using an ultramicrotome (Leica UC7, Leica Microsystems, Wetzlar, Germany) and collected on 150-mesh Formvar-coated copper grids (AZH150, Zhongjing Keyi, Beijing, China). Sections were stained with 3% uranyl acetate (22400, EMS, Hatfield, PA, USA) in a saturated alcohol solution for 8 minutes, followed by 2.7% lead citrate (HD17810, Henan Dinghui Chemical Reagent, Zhengzhou, Henan, China) solution for 8 minutes to enhance contrast.

Control experiments were also performed to confirm the specificity of the precipitation of calcium by potassium pyroantimonate using EGTA chelation. The same embedded block was serially sectioned, inverted on 0.1 M EGTA (pH 8.0), and placed at 60 °C for 30 minutes to specifically chelate Ca^{2+}. After being well rinsed with double distilled water, sections were stained with uranyl acetate and lead citrate and viewed in a transmission electron microscope (JEM-1400, JEOL, Tokyo, Japan).

2.3 Total RNA Extraction and Quality Assessment

Total RNA was extracted from approximately 50 mg of root and leaf tissues of *S. tonkinensis* using the TGuide S96 Magnetic Plant RNA Kit 5 (Polysaccharides & Polyphenolics-rich) (Catalog No. DP862-T5C; Tiangen Biotech, Beijing, China) with a TGuide S96 automatic nucleic acid extraction and purification instrument (Tiangen Biotech). The concentration and purity of the extracted total RNA were assessed using a NanoDrop 2000 spectrophotometer (Thermo Fisher Scientific, Waltham, MA, USA), while RNA integrity was verified using an Agilent 5300 Bioanalyzer (Agilent Technologies, Santa Clara, CA, USA). All RNA samples used for subsequent experiments met the following criteria: OD260/280 of 2.0–2.2, concentration greater than 85 ng/μL, and RNA Quality Number (RQN) exceeding 6.0, indicating good RNA purity.

2.4 cDNA Synthesis

First-strand cDNA was synthesized from 1 μg of total RNA using the HiScript Q RT SuperMix for qPCR (+gDNA wiper) kit (R223-01, Vazyme Biotech Co., Ltd., Nanjing, China). Genomic DNA removal and reverse transcription were conducted according to the manufacturer's instructions. Briefly, the reaction mixture was incubated at 42 °C for 5 minutes for genomic DNA removal, followed by reverse transcription at 50 °C for 15 minutes, and then heated at 85 °C for 2 minutes to inactivate the reverse transcriptase. The resulting cDNA products were diluted with sterile ultrapure water and stored at –20 °C until use.

2.5 Quantitative Real-Time PCR

Quantitative real-time PCR (qRT-PCR) was performed on a QuantStudio™ 5 384-well real-time PCR system (Applied Biosystems, Waltham, MA, USA) in a 10 μL reaction volume comprising: 5 μL of 2 × ChamQ SYBR Color qPCR Master Mix (Q411-02, Vazyme Biotech Co., Ltd.), 0.4 μL of forward primer (5 μM), 0.4 μL of reverse primer (5 μM), 0.2 μL of 50 × ROX Reference Dye 2 (Q411-02, Vazyme Biotech Co., Ltd.), 1 μL of cDNA template, and 3 μL of sterile ultrapure water.

The PCR amplification program included the following steps: pre-denaturation at 95 °C for 3 minutes, denaturation at 95 °C for 5 seconds, and annealing/extension at 55 °C for 30 seconds, across of 40 cycles. A melting curve analysis was performed post-reaction to confirm the specificity of the amplified products.

This study analyzed a total of 14 target genes. Primers were designed and synthesized by Shanghai Majorbio Biopharm Technology Co., Ltd. The specificity of all primers was validated through conventional PCR and melting curve analysis. *Actin* of *S. tonkinensis* served as the internal reference gene, with relative expression levels of target genes calculated using the $2^{-\Delta\Delta Ct}$ method. The primer sequences employed for qRT-PCR are listed in Table 1.

2.6 Statistical Analysis

All data are presented as means ± standard error (SE) derived from three independent biological replicates. Statistical comparisons among multiple groups were conducted using one-way analysis of variance (ANOVA). A significance threshold of $p < 0.05$ was considered statistically significant, while $p < 0.01$ was regarded as extremely significant. All statistical analyses were conducted using SPSS Statistics version 26.0 (IBM Corp., Armonk, NY, USA).

3. Results

3.1 Effects of Different Calcium Channel Blockers on Ca^{2+} Distribution in S. tonkinensis Leaves

Combining the potassium pyroantimonate precipitation technique with transmission electron microscopy (TEM), Ca^{2+} was visualised *in situ* as black flocculent or irregular granular deposits (Fig. 1a). To verify the specificity of the precipitation signal, samples treated with potassium pyroantimonate were exposed to the specific Ca^{2+} chelator EGTA. The black deposits vanished, and plaques were found to be clear, as shown in Fig. 1b. This control experiment confirmed the above observation that the black particles are in fact Ca^{2+} fixed by potassium pyroantimonate. This method is thus an accurate and specific way of reflecting the *in situ* distribution of Ca^{2+}.

Based on these validations, the effects of different calcium channel blocker treatments on Ca^{2+} distribution in *S. tonkinensis* leaves were further analyzed, with results presented in Fig. 2.

R0 (Control treatment): After 20 days, Ca^{2+} signals were predominantly enriched in the cell wall, with no significant deposition observed in the vacuole (Fig. 2a). At 40 and 60 days, the Ca^{2+} distribution pattern remained stable, primarily localized extracellularly, with sparse signals in the cytoplasm and clearly visible organellar structures (Fig. 2b,c).

R1 ($LaCl_3$ treatment): At 20 days, Ca^{2+} was distributed extracellularly (Fig. 2d). At 40 days, intracellular Ca^{2+} signals intensified, with increased granule accumulation in the cytoplasm and a tendency toward aggregation. Deposits began to appear in the vacuole, while extracellular signals diminished (Fig. 2e). At 60 days, cells exhibited plasmolysis, intracellular Ca^{2+} signals weakened somewhat, and extracellular Ca^{2+} signals gradually intensified (Fig. 2f).

Table 1. Primer sequences used for quantitative real-time PCR (qRT-PCR).

Gene name	Primer name	Forward primer sequence (5′-3′)	Reverse primer sequence (5'-3')
StCa^{2+}-ATPase1	evm.model.4.1484	TGGTTTCCTTAATCCGTTAT	TGATCCCATTGTCTCACA
StCa^{2+}-ATPase4	evm.model.325.2	TACAAAGTGCCTGATGAA	AACCCAGAAACTCCTAAC
StCa^{2+}-ATPase5	evm.model.4.2365	AGATGGAGGGAACTATGC	TCAGGCACTTTGTAATCG
StPLC1	evm.model.4.4545	GATAGGCTAGGTGTAAGGG	GGACAATCAGTTCGTGGG
StPLC2	evm.model.3.333	CCCCATCATACAGGCACT	TGGTCTTCAAGGGTTATT
StCAX1	evm.model.2.6359	GCAAGAAGTCTAGCCTCA	AAGCCATAGTATTCAGCA
StCaM4	evm.model.1.2893	AAACAGATTCGGAGGGAG	TGAGTGAAGGGTAGAAATGG
StCDPK1	evm.model.1.4983	TCCACTCATACAGTGCCTCA	GCAAGCATACAGCAACCC
StCDPK2	evm.model.6.1204	ATCTGGAGTGCTGGAGTA	ATTAGGAGCTTTCTTTGC
StCBL1	evm.model.1.187	GCGTGATCCACAGACTCCT	TCAAATCTAATCCCGAAGACA
StCML3	evm.model.2.915	GTCGGAGGAGGTAAGTCG	TTATCATTCTTCGGCAATCT
StCML5	evm.model.1.4113	AGGAGTTCGGCGAGTTTC	GCAATCACTGAGGGAGCA
StCML9	evm.model.2.1131	ACCATTATCAGTTTCGTCG	TAGCCATAGCAAGCATCA
StCML10	evm.model.4.1585	GCCGAATCAAACCCTAACG	TGATGAAGCCGTCGTGGT
Actin	evm.model.3.5465	CATTGTTCTTAGTGGTGGTT	GAGGGATGCAAGGATTGA

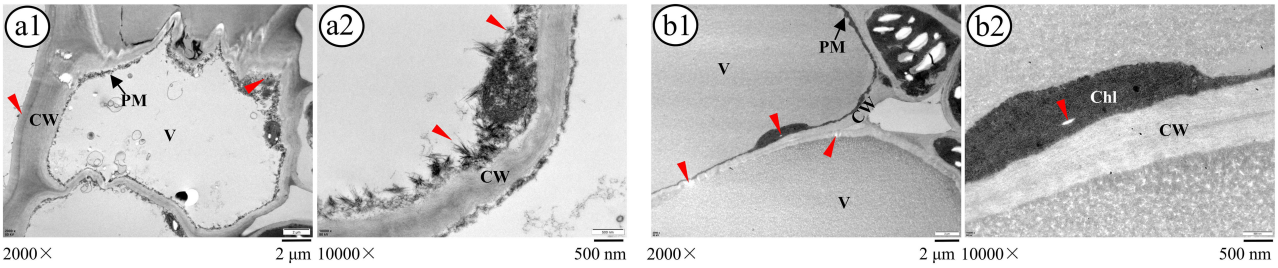

Fig. 1. Distribution of intracellular Ca^{2+} and validation by EGTA treatment. (a1,a2) Black flocculent or irregular particles indicate Ca^{2+} fixed by potassium pyroantimonate (indicated by red arrows). Magnifications: 2000× and 10,000×, respectively. (b1,b2) Ca^{2+} chelated by EGTA appears as transparent empty plaques (indicated by red arrows). Magnifications: 2000× and 10,000×, respectively. CW, cell wall; Chl, chloroplast; PM, plasma membrane; V, vacuole; EGTA, ethylene glycol-bis(β-aminoethyl ether)-N,N,N′,N′-tetraacetic acid. Scale bars: 2 μm (a1,b1; 2000×); 500 nm (a2,b2; 10,000×).

R2 (Na_3VO_4 treatment): At 20 days, Ca^{2+} was notably enriched at the plasma membrane, with scattered granules observed in the cytoplasm (Fig. 2g). At 40 days, some cells exhibited evident plasmolysis, with a small amount of Ca^{2+} present in the cytoplasm and partial deposition visible in and around the vacuole (Fig. 2h). At 60 days, the density of Ca^{2+} in the cytoplasm increased, displaying a more concentrated distribution with localized small patchy aggregates (Fig. 2i).

R3 (EGTA treatment): At 20 days, the overall cellular structure remained intact, with sporadic intracellular Ca^{2+} signals observed (Fig. 2j). At 40 days, cells exhibited pronounced plasmolysis, with persistent intracellular Ca^{2+} signals, and a clear presence of extracellular and membrane-associated Ca^{2+} signals (Fig. 2k). At 60 days, plasmolysis persisted, and both intracellular and extracellular Ca^{2+} signals remained detectable (Fig. 2l).

3.2 Effects of Different Calcium Channel Blockers on Ca^{2+} Distribution in Root Tips of S. tonkinensis

The effects of various calcium channel blocker treatments on Ca^{2+} distribution in the root tips of *S. tonkinensis* are illustrated in Fig. 3.

R0 (Control treatment): At 20 days, Ca^{2+} was predominantly distributed in the cell wall and intercellular spaces (Fig. 3a). By 40 days, Ca^{2+} signals gradually shifted from the extracellular to the intracellular compartment, with an increase in calcium granules observed in the cytoplasm (Fig. 3b). At 60 days, extracellular Ca^{2+} signals intensified further, forming dense deposition bands (Fig. 3c). Overall, the dynamic trend reflected a transition from predominantly extracellular distribution to increased intracellular accumulation, ultimately returning to extracellular localization.

R1 ($LaCl_3$ treatment): At 20 days, Ca^{2+} was primarily located in the intercellular spaces, with a small presence in the cytoplasm (Fig. 3d). At 40 days, while extracellular Ca^{2+} continued to dominate, intracellular Ca^{2+} accumulation increased significantly, with deposits beginning

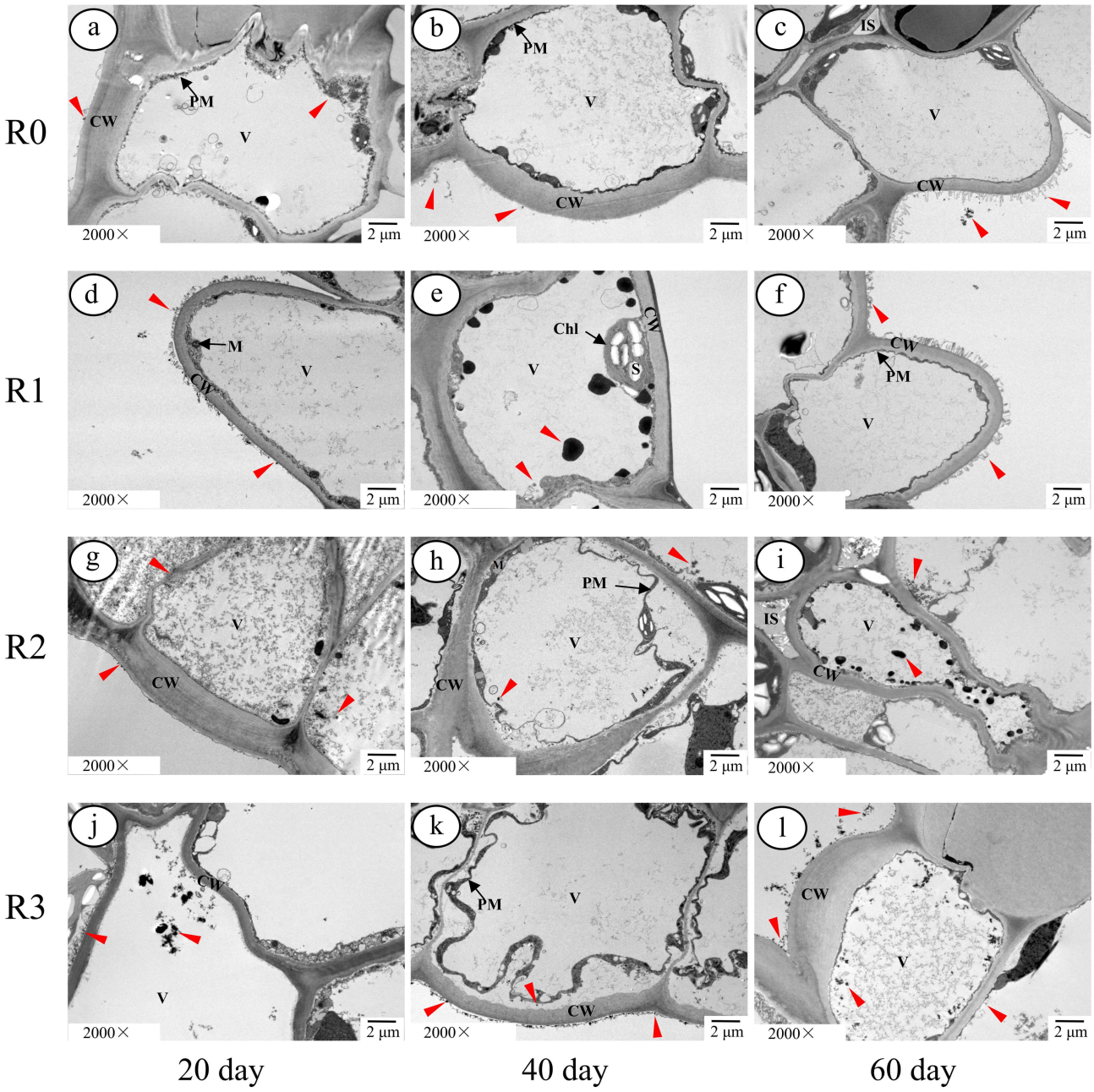

Fig. 2. Observation of Ca^{2+} distribution in mesophyll cells of *S. tonkinensis* leaves under different calcium channel blocker treatments. Black flocculent or irregular particles indicate Ca^{2+} precipitated by potassium pyroantimonate (indicated by red arrows). (a) R0, 20 d (the same micrograph as shown in Fig. 1a1, presented here as the baseline for comparison with treated groups): Ca^{2+} enriched in cell wall, not in vacuole. (b) R0, 40 d: Ca^{2+} mainly extracellular, sparse cytoplasmic signals. (c) R0, 60 d: distribution stable. (d) R1, 20 d: Ca^{2+} extracellular. (e) R1, 40 d: intracellular signals intensified, granules and vacuolar deposits appeared. (f) R1, 60 d: plasmolysis, intracellular signals weakened, extracellular intensified. (g) R2, 20 d: Ca^{2+} enriched at plasma membrane. (h) R2, 40 d: some plasmolysis, Ca^{2+} in cytoplasm and around vacuole. (i) R2, 60 d: cytoplasmic Ca^{2+} increased, patchy aggregates. (j) R3, 20 d: structure intact, sporadic intracellular signals. (k) R3, 40 d: pronounced plasmolysis, clear intra- and extracellular signals. (l) R3, 60 d: plasmolysis persisted, both signals present. CW, cell wall; Chl, chloroplast; M, mitochondrion; IS, intercellular space; PM, plasma membrane; S, starch; V, vacuole. Scale bars: 2 μm (all panels at 2000× magnification).

to appear in the vacuole (Fig. 3e). By 60 days, Ca^{2+} was mainly localized extracellularly, showing broader distribution compared to 40 days, while intracellular Ca^{2+} signals correspondingly diminished (Fig. 3f).

R2 (Na_3VO_4 treatment): At 20 days, Ca^{2+} signals were mainly distributed outside the cells (Fig. 3g). By 40 days, a marked shift toward the intracellular compartment was evident, with clear and dense Ca^{2+} aggregates visible

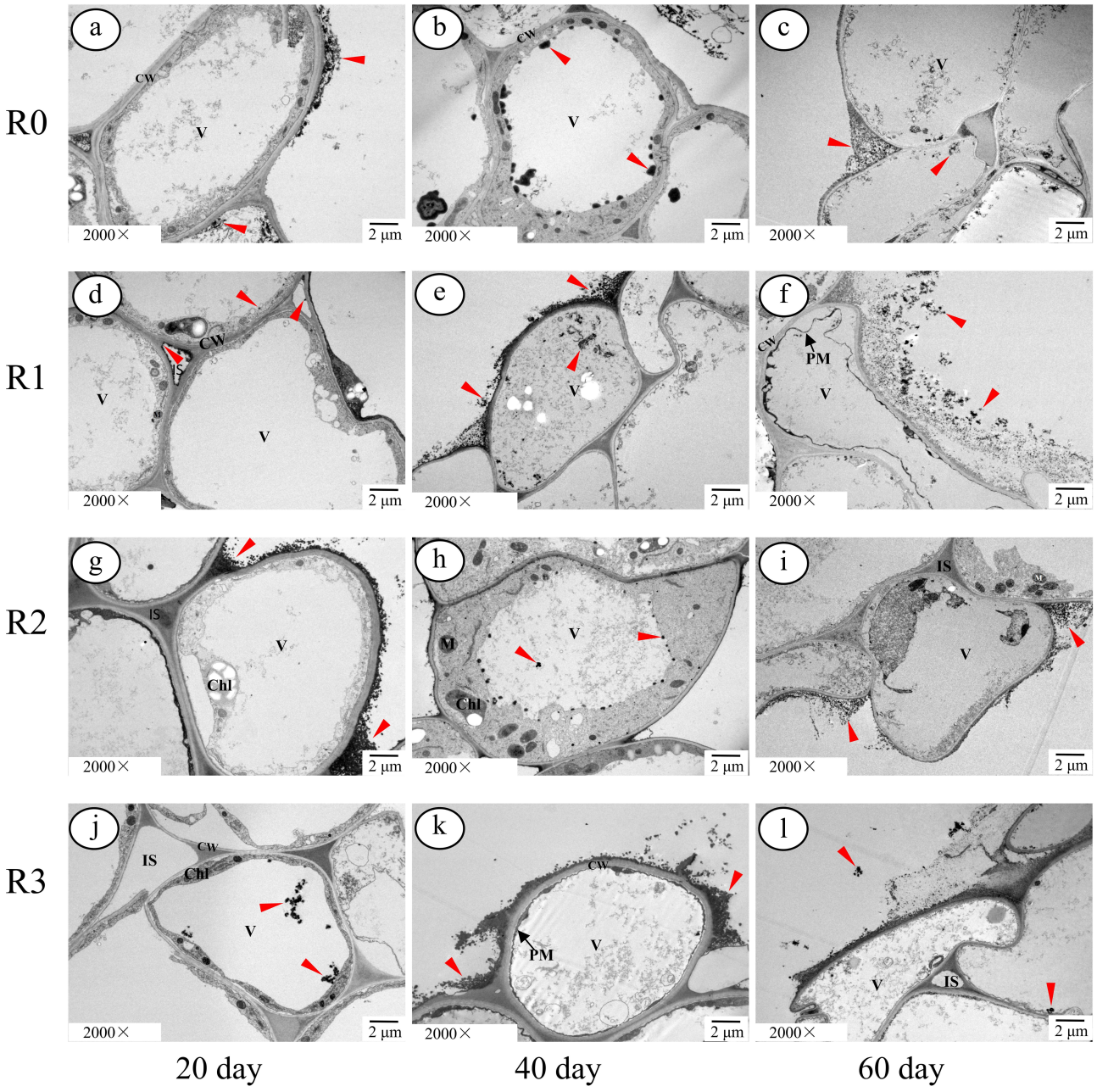

Fig. 3. Observation of Ca^{2+} distribution in root tips of *S. tonkinensis* under different calcium channel blocker treatments. Black flocculent or irregular particles indicate Ca^{2+} precipitated by potassium pyroantimonate (indicated by red arrows). (a) R0, 20 d: Ca^{2+} mainly in cell wall and intercellular spaces. (b) R0, 40 d: Ca^{2+} shifted to cytoplasm with increased granular signals. (c) R0, 60 d: extracellular Ca^{2+} intensified forming dense bands. (d) R1, 20 d: Ca^{2+} primarily in intercellular spaces with a small presence in the cytoplasm. (e) R1, 40 d: extracellular Ca^{2+} dominant, intracellular accumulation increased, vacuolar deposits appeared. (f) R1, 60 d: Ca^{2+} mainly extracellular with broader distribution, intracellular signals diminished. (g) R2, 20 d: Ca^{2+} signals mainly extracellular. (h) R2, 40 d: marked shift to intracellular with dense aggregates in cytoplasm and around vacuolar membrane. (i) R2, 60 d: cytoplasmic Ca^{2+} decreased, extracellular signals intensified, some Ca^{2+} re-transported outward. (j) R3, 20 d: Ca^{2+} predominantly inside vacuole with granular deposits. (k) R3, 40 d: Ca^{2+} shifted to extracellular with deposition in cell wall, intracellular signals weakened. (l) R3, 60 d: Ca^{2+} remained mainly extracellular, cell wall deposition persisted. CW, cell wall; Chl, chloroplast; M, mitochondrion; IS, intercellular space; PM, plasma membrane; S, starch; V, vacuole. Scale bars: 2 μm (all panels at 2000× magnification).

in the cytoplasm and deposits noted around the vacuolar membrane (Fig. 3h). At 60 days, calcium density in the cytoplasm decreased, extracellular Ca^{2+} signals intensified once more, and some Ca^{2+} was re-transported to the extracellular space (Fig. 3i).

R3 (EGTA treatment): At 20 days, Ca^{2+} signals were predominantly located inside the vacuole, with noticeable granular deposits visible within the vacuolar membrane (Fig. 3j). By 40 days, Ca^{2+} signals shifted mainly to the extracellular space, with clear deposition in the cell wall and weakened intracellular Ca^{2+} signals (Fig. 3k). At 60 days, Ca^{2+} signals remained primarily extracellular, and deposition in the cell wall persisted (Fig. 3l).

3.3 Expression Responses of Calcium Signaling Genes in the Leaves of S. tonkinensis to Different Calcium Channel Blockers

To investigate the effects of calcium channel blockers on the expression of genes associated with calcium signaling pathways, 14 calcium signaling-related genes were selected as targets. These genes were previously identified through correlation analysis as significantly correlated with the accumulation of medicinal active components in *S. tonkinensis* [20]. The expression patterns of these 14 genes under different calcium channel blocker treatments were analyzed using qRT-PCR. As illustrated in Fig. 4, treatment with calcium channel blockers led to significant suppression or induction of most examined genes in leaf tissues. The expression of the calcium pump gene *StCa^{2+}-ATPase1* (evm.model.4.1484) was suppressed following R2 (Na_3VO_4) treatment. However, it was significantly upregulated at 60 days under R3 (EGTA) treatment, reaching a relative expression level of 3.4643 (approximately 2-fold that of the control). The expression of the calcium transporter gene *StCAX1* (evm.model.2.6359) was markedly and significantly upregulated under R1 and R2 treatments. Its highest expression level (6.562, approximately 6.6-fold that of the control) was observed under R3 treatment at 20 days. This suggests that when calcium influx or efflux is obstructed, cells may enhance CAX-mediated vacuolar compartmentalization to adapt to changes in cytoplasmic calcium levels. The phospholipase C (PLC) gene *StPLC1* (evm.model.4.4545) was significantly induced under R1 treatment, reaching 2.823 at 20 days (2.8-fold that of the control), but it was suppressed under R2 treatment. On the other hand, *StPLC2* (evm.model.3.333) exhibited variable expression patterns across different treatments, indicating that these two genes may be involved in distinct regulatory pathways in the initiation of calcium signaling in leaves. The calcium-dependent protein kinase (CDPK) genes *StCDPK1* (evm.model.1.4983) and *StCDPK2* (evm.model.6.1204) were generally and significantly suppressed across all blocker treatments. Extremely significant differences were seen between expression levels of *StCDPK2* and its reduction level to as low as 0.1613, which is more than 80% reduction. This suggests that CDPK kinases may be subject to negative feedback regulation of their activity or expression when calcium signaling pathways are impaired.

Calcium-binding protein genes exhibited diverse response patterns. For instance, the calmodulin-like protein (CML) gene *StCML9* (evm.model.2.1131) was significantly upregulated to 4.214 at 40 days under control conditions (R0) but was generally downregulated under blocker treatments. In contrast, the calcineurin B-like protein gene *StCBL1* (evm.model.1.187) showed significant upregulation under R2 treatment (1.4317 at 20 days) but was strongly suppressed under R1 and R3 treatments. These results suggest that different calcium-binding proteins may respond uniquely to distinct types of calcium signaling perturbations.

3.4 Expression Responses of Calcium Signaling Genes in the Roots of S. tonkinensis to Different Calcium Channel Blockers

In contrast to leaves, root tissues exhibited a more pronounced response to calcium channel blockers, with several genes showing significant upregulation (Fig. 5). The expression of the calcium pump gene *StCa^{2+}-ATPase1* (evm.model.4.1484) increased sharply to 3.8540 following 20 days of R3 (EGTA) treatment, approximately 3.9-fold higher than the control (R0). Similarly, the calcium transporter gene *StCAX1* (evm.model.2.6359) was notably upregulated, reaching 4.1830 under R3 treatment at 20 days (approximately 4.2-fold that of the control), confirming its crucial role in Ca^{2+} transport and homeostasis in roots. The PLC gene *StPLC2* (evm.model.3.333) was significantly upregulated under R1 and R3 treatments. It peaked at 2.4190 after 20 days of R3 treatment (approximately 2.4-fold that of the control). This suggests its activation in response to extracellular calcium depletion or plasma membrane channel inhibition. The CDPK gene *StCDPK1* (evm.model.1.4983) displayed a significant upregulation trend under R1 and R3 treatments. Its expression reached 2.3493 after 60 days of R1 treatment (approximately 1.7-fold that of the control). This suggests that CDPK may play a role as a signaling component in roots, potentially contributing to adaptive responses to calcium signaling. Notably, the expression of the calmodulin-like gene *StCML9* (evm.model.2.1131) surged dramatically after 20 days of R1 treatment. It reached 11.6620 (approximately 11.7-fold that of the control). It remained elevated across multiple time points under both R1 and R2 treatments (e.g., 8.7243 in R1-2-G), with extremely significant differences observed. This suggests that *StCML9* may serve as a sensor or buffer in roots. It appears to be potentially involved in responding to interference in calcium signaling pathways, particularly under plasma membrane calcium channel and calcium pump inhibition. Additionally, both *StCML3* (evm.model.2.915) and *StCML5* (evm.model.1.4113) exhibited significant upregulation under R3 treatment.

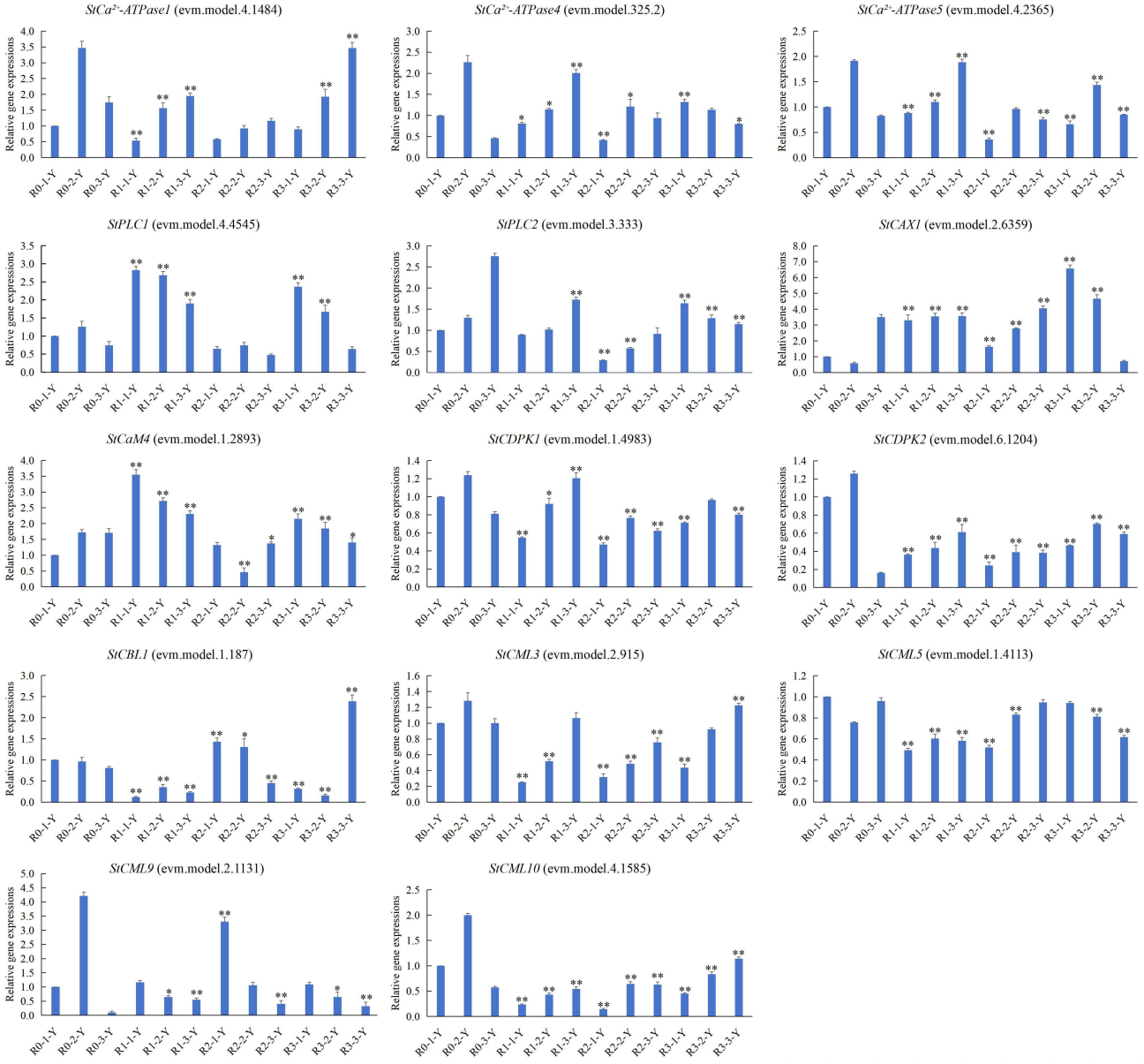

Fig. 4. Expression profiles of calcium signaling-related genes in *S. tonkinensis* leaves in response to different calcium channel blocker treatments. X-axis labels represent treatment groups at different time points: "1-Y" indicates leaves harvested at 20 days post-treatment, "2-Y" indicates leaves harvested at 40 days post-treatment, and "3-Y" indicates leaves harvested at 60 days post-treatment. Data are presented as means ± standard error (SE) (n = 3 biological replicates). * $p < 0.05$ and ** $p < 0.01$ indicate significant and extremely significant differences, respectively, compared to the corresponding R0 control at the same time point (one-way analysis of variance (ANOVA)). R0, control (no blocker); R1, 50 μM $LaCl_3$ (lanthanum chloride); R2, 50 μM Na_3VO_4 (sodium orthovanadate); R3, 0.5 mM EGTA.

4. Discussion

4.1 Differential Responses of Leaves and Roots to Calcium Signaling Perturbation

Under control conditions, the distinct Ca^{2+} distribution patterns in leaves and roots (Figs. 2a–c,3a–c) suggest fundamentally different calcium homeostasis strategies: leaves maintain a stable extracellular Ca^{2+} pool in the cell wall [22], whereas roots exhibit dynamic spatiotemporal Ca^{2+} redistribution. This divergence likely reflects the root's more active role as the primary absorptive organ, continuously sensing and responding to fluctuating external ion concentrations [6,23].

The differential susceptibility of leaves and roots to calcium signaling perturbation was most evident under $LaCl_3$ treatment. Leaf cells, when plasma membrane Ca^{2+} influx was blocked [24], relied heavily on vacuolar sequestration as a compensatory mechanism [25]. However, this compensation proved insufficient, ultimately leading

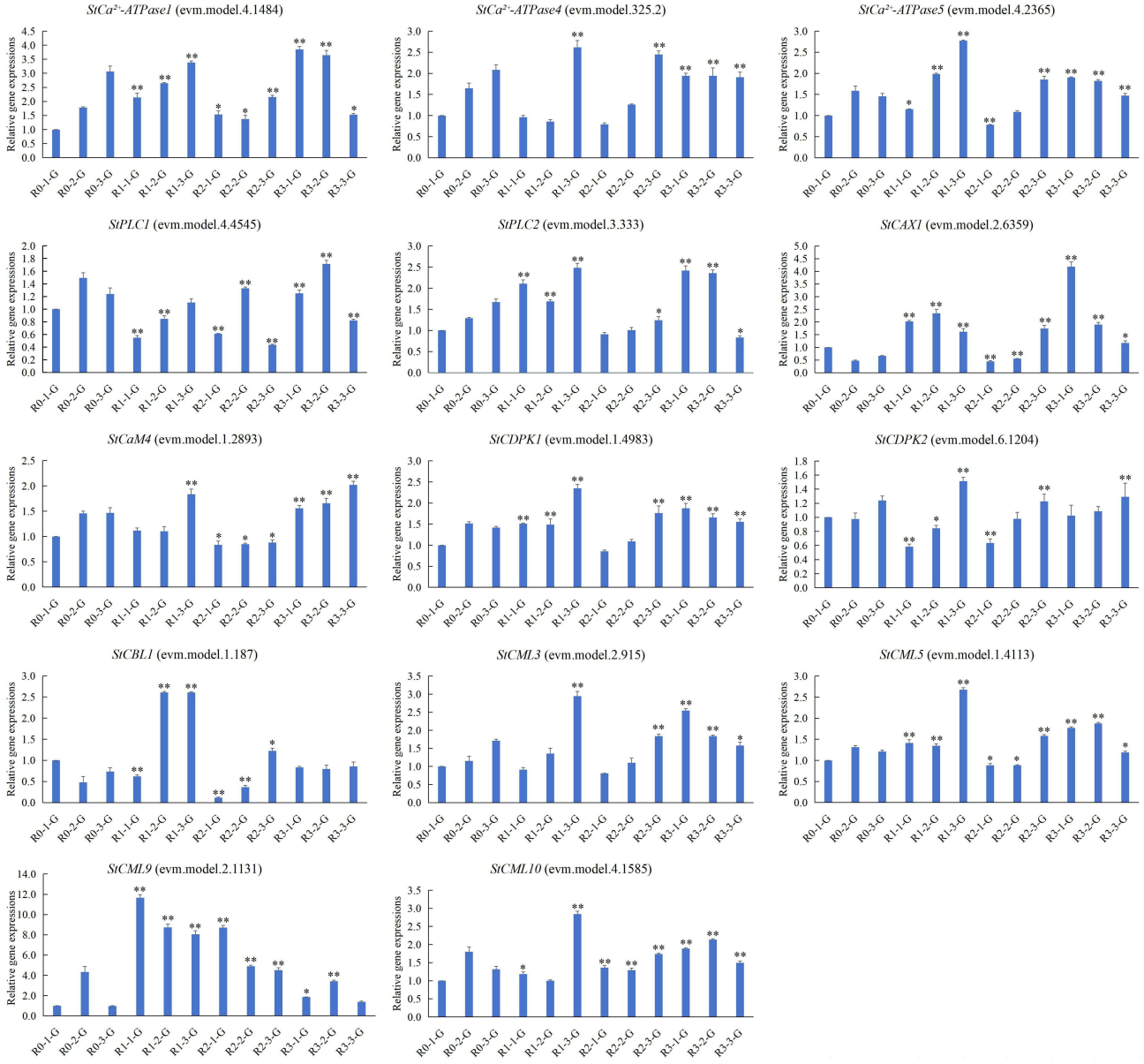

Fig. 5. Expression profiles of calcium signaling-related genes in *S. tonkinensis* roots in response to different calcium channel blocker treatments. X-axis labels represent treatment groups at different time points: "1-G" indicates roots harvested at 20 days post-treatment, "2-G" indicates roots harvested at 40 days post-treatment, and "3-G" indicates roots harvested at 60 days post-treatment. Data are presented as means ± SE (n = 3 biological replicates). * $p < 0.05$ and ** $p < 0.01$ indicate significant and extremely significant differences, respectively, compared to the corresponding R0 control at the same time point (one-way ANOVA). R0, control (no blocker); R1, 50 μM $LaCl_3$; R2, 50 μM Na_3VO_4; R3, 0.5 mM EGTA.

to plasmolysis (Fig. 2e,f). In contrast, roots exhibited only transient intracellular Ca^{2+} accumulation and subsequently re-established extracellular deposition (Fig. 3e,f), indicating more efficient Ca^{2+} efflux or compartmentalization mechanisms. This tissue-specific difference may reflect evolutionary adaptation of roots to the complex and variable soil environment [26]. Consistent with this interpretation, study in hybrid white poplar (*Populus alba* × *P. glandulosa*) has shown that $LaCl_3$ treatment attenuates Ca^{2+} signals and induces tension wood formation, underscoring the critical role of plasma membrane calcium channels in normal cellular development [27].

The response to Na_3VO_4 treatment further supports this organ-specific paradigm. In leaves, inhibition of H^+-ATPase activity led to plasma membrane Ca^{2+} enrichment, cytoplasmic overload, and plasmolysis (Fig. 2g–i). This indicates that suppression of H^+-ATPase activity impairs the cell's ability to drive Ca^{2+} efflux, leading to cytoplasmic Ca^{2+} accumulation and resulting cellular damage [28,29,30]. In contrast, roots exhibited a recovery trend

characterized by initial Ca^{2+} influx followed by subsequent efflux under Na_3VO_4 treatment (Fig. 3g–i). This suggests that roots may partially compensate for the loss of H^+-ATPase function by activating alternative calcium transport systems, such as upregulation of vacuolar CAX [31] and activation of organellar calcium pumps [32,33].

Under EGTA treatment, the contrast between tissues was particularly striking. Leaves exhibited persistent plasmolysis (Fig. 2j–l), indicating limited adaptation to extracellular calcium depletion, consistent with previous reports that EGTA compromises stress tolerance [34,35]. Remarkably, root cells adapted by initially sequestering Ca^{2+} in the vacuole, then transporting it outward for cell wall deposition (Fig. 3j–l). These dynamic responses suggest that root cells may achieve adaptive Ca^{2+} homeostasis redistribution by coordinating the release of internal calcium stores, activating efflux pathways, and enhancing cell wall binding, potentially reflecting a strong capacity for calcium resource reallocation and structural adaptation under calcium stress [36].

It is important to acknowledge that the pharmacological inhibitors used in this study are not entirely specific. $LaCl_3$ can affect multiple cation channels beyond plasma membrane Ca^{2+} channels; Na_3VO_4 inhibits various P-type ATPases and phosphatases beyond Ca^{2+}-ATPase; and EGTA may indirectly alter membrane integrity and ion balance. Therefore, while the observed phenotypes are consistent with the targeted calcium signaling pathways, the possibility of off-target contributions cannot be excluded. The conclusions drawn from these experiments should be considered correlative rather than definitive.

4.2 Tissue-Specific Expression Patterns of Calcium Signaling-Related Genes

The transcriptional responses of different tissues further corroborated the observed tissue specificity. The calcium pump gene *StCa^{2+}-ATPase1* and the calcium transporter gene *StCAX1* exhibited markedly distinct expression patterns in leaves and roots. In leaves, *StCAX1* was highly induced by $LaCl_3$ and Na_3VO_4 (Fig. 4), which directly correlates with vacuolar Ca^{2+} deposition (Fig. 2e,h). These results suggest that when plasma membrane Ca^{2+} influx is impaired, leaves may activate *StCAX1* to sequester cytoplasmic Ca^{2+} into the vacuole, potentially buffering against calcium overload. CAX family proteins play critical roles in calcium signal clearance and osmotic regulation [37,38]. In roots, the expression of *StCAX1* and *StCa^{2+}-ATPase1* was rapidly upregulated during early EGTA treatment (Fig. 5), coinciding with vacuolar Ca^{2+} deposition (Fig. 3j). Moreover, *StCa^{2+}-ATPase1* exhibited a faster response in roots, suggesting that root cells necessitate immediate activation of *Ca^{2+}-ATPase* to cope with extracellular calcium depletion [7,34].

The phosphoinositide signaling pathway is a major pathway in which PLC plays an important role and hydrolyzes phosphatidylinositol to inositol trisphosphate (IP_3), which in turn causes release of Ca^{2+} from internal stores, amplifying the calcium signals [39,40]. In the present study, *StPLC1* was mostly responsive to $LaCl_3$ in leaves (Fig. 4), whereas *StPLC2* was responsive to both $LaCl_3$ and EGTA in roots (Fig. 5). This suggests that the roots have an enhanced PLC-mediated ability to mobilize internal Ca^{2+} stores, and this is in line with their high adaptability in the extracellular calcium deprivation (Fig. 3j–l). A recent study in carrot has been able to identify the PI-PLC-GLRs-Ca^{2+} pathway, which further emphasizes the importance of PLC in the calcium signal amplification process [41].

The response of CDPKs also exhibited tissue specificity. In leaves, all blocker treatments strongly suppressed the expression of *StCDPK1* and *StCDPK2* (Fig. 4), potentially reflecting negative feedback regulation in response to impaired calcium signaling [42]. This aligns with findings from Liese et al. [43], who developed a CDPK-FRET reporter system that demonstrated CDPKs act as calcium signal decoders responsive to specific calcium signatures. In contrast, *StCDPK1* was significantly upregulated in roots under $LaCl_3$ and EGTA treatment (Fig. 5), suggesting that *CDPK1* may function as a central hub initiating adaptive responses in roots [44,45].

CMLs serve as key calcium sensors in plants, playing significant roles in regulating various developmental processes and stress responses [46,47]. In this study, *StCML9* exhibited extremely high expression in roots under $LaCl_3$ and Na_3VO_4 treatments (up to 11.7-fold relative to the control, Fig. 5), with its expression dynamics closely linked to fluctuations in Ca^{2+} levels. This suggests that *StCML9* may serve as a root-specific calcium sensor or buffer, potentially detecting perturbations in plasma membrane calcium channel or pump function, and possibly contributing to protective responses such as vacuolar compartmentalization (Fig. 3e) and calcium efflux (Fig. 3f) [47]. Additionally, *StCML3* and *StCML5* were significantly upregulated under EGTA treatment, implying that different CMLs may respond to distinct types of calcium signaling perturbation, thereby highlighting the functional diversification within the CML family.

4.3 Integrated Analysis of Cytological Phenotypes and Molecular Responses

By systematically correlating the subcellular Ca^{2+} distribution patterns induced by pharmacological blockade with corresponding gene expression changes, this study demonstrated a strong temporal concordance between gene expression dynamics and shifts in calcium distribution, providing compelling evidence for the calcium homeostasis regulatory network.

Under $LaCl_3$ treatment, the exceptionally high expression of *StCML9* in roots closely aligned with intracellular Ca^{2+} fluctuations (Fig. 3d–f). *StCML9* upregulation par-

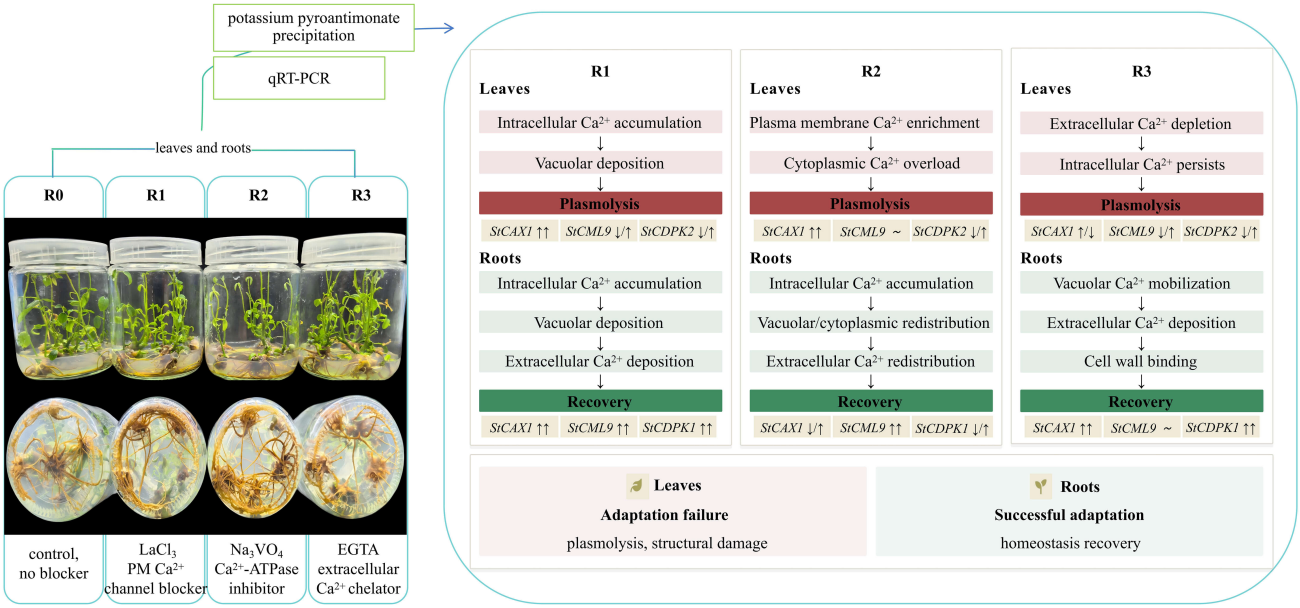

Fig. 6. Proposed model of organ-specific calcium homeostasis strategies in *S. tonkinensis* under calcium signaling perturbation. The model summarizes the differential responses of leaves and roots to three pharmacological treatments: R1 ($LaCl_3$, a plasma membrane Ca^{2+} channel blocker), R2 (Na_3VO_4, a Ca^{2+}-ATPase inhibitor), and R3 (EGTA, an extracellular Ca^{2+} chelator). Arrows indicate the direction of Ca^{2+} movement. Gene expression changes are indicated with ↑ for upregulation, ↓ for downregulation, and ~ for variable/no consistent trend. *S. tonkinensis* may achieve calcium stress adaptation through organ-specific calcium distribution and transcriptional reprogramming.

alleled Ca^{2+} accumulation. Sustained *StCML9* expression matched vacuolar Ca^{2+} deposition. The subsequent decline in its expression corresponded to Ca^{2+} efflux recovery. This temporal alignment suggests a potential role for *StCML9* in calcium sensing or buffering, possibly contributing to the regulation of cytoplasmic calcium fluctuations. Simultaneously, $LaCl_3$-induced intracellular calcium accumulation paralleled *StCAX1* upregulation (Fig. 4), further supporting the role of vacuolar compartmentalization in response to plasma membrane calcium channel blockade.

In the later stages of Na_3VO_4 treatment, cytoplasmic Ca^{2+} density in leaves increased, forming localized patchy aggregates (Fig. 2i). However, *StCa^{2+}-ATPase1* expression remained unchanged (Fig. 4). This suggests the activation of alternative Ca^{2+} efflux systems, such as mitochondrial or endoplasmic reticulum calcium pumps [32,33]. This observation is consistent with results indicating that cells are able to maintain ion homeostasis via other pathways when the activity of the H^+-ATPase is blocked [9].

During the early phase of EGTA treatment, the expression of *StCAX1* and *StCa^{2+}-ATPase1* was sharply upregulated in roots (Fig. 5), coinciding with vacuolar Ca^{2+} deposition (Fig. 3j). This suggests that when extracellular calcium is chelated and depleted, root cells may activate vacuolar calcium transport systems to sequester cytoplasmic Ca^{2+} and maintain calcium homeostasis [31,37]. Later, as Ca^{2+} was transported outward and deposited in the cell wall (Fig. 3k,l), gene expression levels declined, suggesting that cells may have reached a new calcium homeostasis equilibrium. This spatiotemporal regulatory pattern is consistent with the "calcium signal encoding-decoding-response" model [48,49].

Leaves and roots exhibited strikingly different gene expression-phenotype associations in response to the same blocker. For example, leaves showed stable plasmolysis under EGTA treatment (Fig. 2j–l), and *StCAX1*, *StCML9*, and other genes were strongly up-regulated during this time in the roots (Fig. 5). This shows that the molecular basis of the calcium homeostasis regulation in tissues is different, probably because roots as primary absorptive organs have adapted to the complex and variable soil environment with more flexible mechanisms of calcium homeostasis [27,49].

5. Limitations

Although this study has a number of important implications, there are several limitations that should be noted. The first is that the pharmacological inhibitors utilized (namely $LaCl_3$, Na_3VO_4, and EGTA) are not completely specific, and thus may exhibit off-target effects. Second, our conclusions are based primarily on transcript abundance and subcellular Ca^{2+} localization using a qualitative method (potassium pyroantimonate-TEM). Direct quantitative measurements of calcium concentration, such as atomic absorption spectroscopy or calcium-sensitive fluorescent probes, were not performed. Therefore, the observed phenotypes may not be solely explained by the targeted cal-

cium signaling pathways, and the correlative nature of the data does not give us a complete picture of causality. Future studies employing complementary quantitative approaches and genetic validation will be valuable to further validate the findings presented here.

6. Conclusion

The correlative evidence presented in this study suggests that the leaves and roots of *S. tonkinensis* may employ distinct strategies to maintain calcium homeostasis under prolonged calcium signaling perturbation (Fig. 6). Leaves appear to primarily rely on stable extracellular calcium pools and vacuolar compartmentalization, whereas roots exhibit a dynamic calcium resource reallocation pattern, potentially involving candidate genes such as *StCAX1*, *StCML9*, and *StCDPK1*. By integrating cytological observations with molecular expression profiling, this study reveals a correlation between calcium perturbation phenotypes and gene expression changes, suggesting a potential connection. These findings offer important candidate genes for future functional studies to determine whether these genes play direct roles in calcium homeostasis. Such studies may ultimately lay a theoretical foundation for genetic enhancement.

Abbreviations

$LaCl_3$, Lanthanum chloride; Na_3VO_4, Sodium orthovanadate; EGTA, Ethylene glycol-bis(β-aminoethyl ether)-N,N,N′,N′-tetraacetic acid; MS, Murashige and Skoog medium; CAX, Cation/H^+ Exchanger; CBL, Calcineurin B-Like Protein; CDPK, Calcium-Dependent Protein Kinase; CML, Calmodulin-Like Protein; PLC, Phospholipase C; qRT-PCR, Quantitative Real-Time PCR; TEM, Transmission Electron Microscopy.

Disclosure

The paper is listed as, "Effects of Calcium Channel Blockers on Intracellular Calcium Distribution and Expression of Calcium Signaling-Related Genes in *Sophora tonkinensis*" as a preprint on Research Square at: https://www.researchsquare.com/article/rs-9492547/v1.

Availability of Data and Materials

The raw data supporting the conclusions of this article will be made available by the authors on request.

Author Contributions

YL: Formal analysis, Validation, Data curation, Funding Acquisition, Writing-original draft preparation. SQ: Methodology, Resources. GW: Performed the data analysis and contributed to the interpretation of the results. YH: Investigation. HH: Data curation. FW: Conceptualization, Supervision, Writing-review and editing. All authors have read and agreed to the final version of the manuscript. All authors contributed to editorial changes in the manuscript. All authors have participated sufficiently in the work and agreed to be accountable for all aspects of the work.

Ethics Approval and Consent to Participate

Not applicable.

Acknowledgment

Not applicable.

Funding

This research was funded by the National Natural Science Foundation of China (82260747 and 82560744); Natural Science Foundation of Guangxi (2025GXNSFAA069971).

Conflicts of Interest

The authors declare no conflicts of interest.

Declaration of AI and AI-Assisted Technologies in the Writing Process

During the preparation of this work, the authors used DeepSeek to refine the manuscript's English language. The authors reviewed and edited the AI-generated output and take full responsibility for the final content.

References

[1] Zheng Y, Zhan Q, Shi T, Liu J, Zhao K, Gao Y. The nuclear transporter SAD2 plays a role in calcium- and H_2 O_2 -mediated cell death in Arabidopsis. The Plant Journal : for Cell and Molecular Biology. 2020; 101: 324–333. https://doi.org/10.1111/tpj.14544

[2] Bouvie F, Pereira DT, Ouriques LC, Puerari RC, Matias WG, Hayashi L, et al. Effects of extracellular calcium ion on the germination of Gelidium floridanum (Rhodophyta, Gelidiales) tetraspores. Micron (Oxford, England : 1993). 2026; 201: 103942. https://doi.org/10.1016/j.micron.2025.103942

[3] Li L, Gazzo D, Saad SM, Larson NJ, Kim ES, Kumar N, et al. Rules of life at the interface of calcium signaling and mechanobiology. APL Bioengineering. 2025; 9: 041504. https://doi.org/10.1063/5.0284022

[4] Zhang W, Kumar N, Helwig JR, Hoerter A, Iyer-Pascuzzi AS, Umulis DM, et al. Local traveling waves of cytosolic Ca^{2+} elicited by defense signals or wounding are propagated by distinct mechanisms in *Arabidopsis*. Science Signaling. 2025; 18: eadw2270. https://doi.org/10.1126/scisignal.adw2270

[5] Gupta V, Roy A, Tripathy BC. Signaling events leading to red-light-induced suppression of photomorphogenesis in wheat (Triticum aestivum). Plant & Cell Physiology. 2010; 51: 1788–1799. https://doi.org/10.1093/pcp/pcq139

[6] Chen J, Mo Y, Xu H. Effect of calcium signaling reagent on negative phototropism of rice seminal roots. Chinese Journal of Rice Science. 2013; 27: 265–272. https://doi.org/10.3969/j.issn.1001-7216.2013.03.006

[7] Qi N, Wang N, Hou X, Li Y, Liao W. Involvement of Calcium and Calmodulin in NO-Alleviated Salt Stress in Tomato Seedlings. Plants (Basel, Switzerland). 2022; 11: 2479. https://doi.org/10.3390/plants11192479

[8] Singh P, Sharma S, Prasad V. Verapamil, a calcium chan-

nel blocker, induces systemic antiviral resistance in susceptible plants. Journal of Phytopathology. 2011; 159: 127–129. https://doi.org/10.1111/j.1439-0434.2010.01738.x

[9] Zhou S, Wang W, Wang P, Ma H, Li W. The role of reactive oxygen species in regulation of the plasma membrane H+-ATPase activity in Masson pine (Pinus massoniana Lamb.) roots responding to acid stress. Tree Physiology. 2024; 44: tpae083. https://doi.org/10.1093/treephys/tpae083

[10] Hepler PK. Calcium: a central regulator of plant growth and development. The Plant Cell. 2005; 17: 2142–2155. https://doi.org/10.1105/tpc.105.032508

[11] WU Q, NI Q, Que YC, Huang W. Calcium and calmodulin involve in mycorrhizal and root development in trifoliate orange colonized by Rhizophagus intraradices. Notulae Botanicae Horti Agrobotanici Cluj-Napoca. 2014; 42: 380–385. https://doi.org/10.15835/nbha4229635

[12] Zhang Q, Song T, Guan C, Gao Y, Ma J, Gu X, et al. OsANN4 modulates ROS production and mediates Ca^{2+} influx in response to ABA. BMC Plant Biology. 2021; 21: 474. https://doi.org/10.1186/s12870-021-03248-3

[13] Ma C, Pei ZQ, Zhu Q, Chai CH, Xu TT, Dong CY, et al. Melatonin-mediated low-temperature tolerance of cucumber seedlings requires Ca^{2+}/CPKs signaling pathway. Plant Physiology and Biochemistry : PPB. 2024; 214: 108962. https://doi.org/10.1016/j.plaphy.2024.108962

[14] Yang R, Zhang R, Yang W, Guan X. Effects of Ca2+ messenger on cold-resistance physiology of Euon ymus japonicus 'CuZhi'leaves. Journal of Beijing University of Agriculture. 2012; 27: 20–24. https://doi.org/10.3969/j.issn.1002-3186.2012.04.007 (In Chinese)

[15] Lu WL, Xie XG, Ai HW, Wu HF, Dai YY, Wang LN, et al. Crosstalk between H2O2 and Ca2+ signaling is involved in root endophyte-enhanced tanshinone biosynthesis of Salvia miltiorrhiza. Microbiological Research. 2024; 285:127740. https://doi.org/10.1016/j.micres.2024.127740.

[16] Chi Z, Dai Y, Cao S, Wei Y, Shao X, Huang X, et al. Exogenous calcium chloride (CaCl2) promotes γ-aminobutyric acid (GABA) accumulation in fresh-cut pears. Postharvest Biology and Technology. 2021; 174: 111446. https://doi.org/10.1016/J.POSTHARVBIO.2020.111446

[17] Cao Y, Wang Y, Gui C, Nguvo KJ, Ma L, Wang Q, et al. Beneficial Rhizobacterium Triggers Induced Systemic Resistance of Maize to Gibberella Stalk Rot via Calcium Signaling. Molecular Plant-microbe Interactions : MPMI. 2023; 36: 516–528. https://doi.org/10.1094/MPMI-08-22-0173-R

[18] Zhao S, Du M, Guo S, Zhang S, Zhao H, Zhao C. Calcium regulates reactive oxygen species and endophytic bacteria to enhance rice resistance to sheath blight. Scientia Agricultura Sinica. 2025; 58: 2145–2161. https://doi.org/10.3864/j.issn.0578-1752.2025.11.006

[19] Liang Y, Wei F, Qin S, Li M, Hu Y, Lin Y, et al. Sophora tonkinensis: response and adaptation of physiological characteristics, functional traits, and secondary metabolites to drought stress. Plant Biology (Stuttgart, Germany). 2023; 25: 1109–1120. https://doi.org/10.1111/plb.13578

[20] Qiao Z, Fan ZT, Chen LY, Li LX, Wei F, Qin SS, et al. Integrated Omic Analyses Reveal Module Networks Regulating Growth and Bioactive Component Synthesis of *Sophora tonkinensis* via Calcium Modulation. Plants (Basel, Switzerland). 2026; 15: 133. https://doi.org/10.3390/plants15010133

[21] Murashige T, Skoog FA. A revised medium for rapid growth and bio assays with tobacco tissue cultures. Physiol Plant. 1962; 15: 473–497. https://doi.org/10.1111/j.1399-3054.1962.tb08052.x

[22] Gai W, Liu C, Yang M, Li F, Xin H, Gai S. Calcium signaling facilitates chilling- and GA- induced dormancy release in tree peony. Frontiers in Plant Science. 2024; 15: 1362804. https://doi.org/10.3389/fpls.2024.1362804

[23] Bonza MC, Loro G, Behera S, Wong A, Kudla J, Costa A. Analyses of Ca2+ accumulation and dynamics in the endoplasmic reticulum of Arabidopsis root cells using a genetically encoded Cameleon sensor. Plant Physiology. 2013; 163: 1230–1241. https://doi.org/10.1104/pp.113.226050

[24] Weng X, Li H, Zhou Y, Wang H, Feng J, Yu S, et al. Inhibition of photosynthesis in Quercus acutissima seedlings by LaCl3 through calcium signaling regulation. Forests. 2025; 16: 1553. https://doi.org/10.3390/f16101553

[25] Sakai-Wada A, Yagi S. Ultrastructural studies on the Ca2+ localization in the dividing cells of the maize root tip. Cell Structure and Function. 1993; 18: 389–397. https://doi.org/10.1247/csf.18.389

[26] Tian W, Wang C, Gao Q, Li L, Luan S. Calcium spikes, waves and oscillations in plant development and biotic interactions. Nature Plants. 2020; 6: 750–759. https://doi.org/10.1038/s41477-020-0667-6

[27] An Y, Qu MQ, Geng Y, Jiao X, Song XQ, Zhao ST, et al. Calcium signaling mediated by glutamate receptor-like protein PagGLR3.3 is involved in tension wood induction in poplar. Journal of Integrative Plant Biology. 2026; 68: 1349–1366. https://doi.org/10.1111/jipb.70158

[28] Luo X, Bi H, Su K, Liu Y, Li Y, Zhang X. CsSAD1-silenced in tea leaves impairs drought tolerance by decreasing plasma membrane H+-ATPase activity. Tree Physiology. 2025; 45: tpaf043. https://doi.org/10.1093/treephys/tpaf043

[29] Zhou S, Wang P, Ding Y, Xie L, Li A. Modification of plasma membrane H+-ATPase in Masson pine (Pinus massoniana Lamb.) seedling roots adapting to acid deposition. Tree Physiology. 2022; 42: 1432–1449. https://doi.org/10.1093/treephys/tpac015

[30] Kinoshita T, Nishimura M, Shimazaki K. Cytosolic Concentration of Ca2+ Regulates the Plasma Membrane H+-ATPase in Guard Cells of Fava Bean. Plant Cell. 1995; 7: 1333–1342. https://doi.org/10.1105/tpc.7.8.1333

[31] Chandan K, Gupta M, Ahmad A, Sarwat M. P-type calcium ATPases play important roles in biotic and abiotic stress signaling. Planta. 2024; 260: 37. https://doi.org/10.1007/s00425-024-04462-7

[32] Pirayesh N, Giridhar M, Ben Khedher A, Vothknecht UC, Chigri F. Organellar calcium signaling in plants: An update. Biochimica et Biophysica Acta. Molecular Cell Research. 2021; 1868: 118948. https://doi.org/10.1016/j.bbamcr.2021.118948

[33] Steiner P, Zierler S. Inter-Organellar Ca^{2+} Homeostasis in Plant and Animal Systems. Cells. 2025; 14: 1204. https://doi.org/10.3390/cells14151204

[34] Zhang Y, Liu GM, Wang ZF, Zhang AM, Yang YL. Exogenous calcium-alleviating effect on sodium salt-induced phytotoxicity associated with changes in photosynthetic characteristics of wheat seedlings. Photosynthetica. 2024; 62: 16–26. https://doi.org/10.32615/ps.2023.039

[35] Zhao W, Zhang X, Liang F, Zhang G, Xu J, Li Z. Effects of calcium ions and their inhibitors on the morphogenesis of cucumber seedlings under salt stress. Northern Horticulture. 2024: 1–8. https://doi.org/10.11937/bfyy.20240867 (In Chinese)

[36] Wang T, Chen X, Ju C, Wang C. Calcium signaling in plant mineral nutrition: From uptake to transport. Plant Communications. 2023; 4: 100678. https://doi.org/10.1016/j.xplc.2023.100678

[37] Hao X, Zhao X, Xie Z, Jin X, Li S, Wu S, et al. The rice cation/calcium exchanger OsCCX2 is involved in calcium signal clearance and osmotic tolerance. Journal of Integrative Plant Biology. 2025; 67: 2897–2911. https://doi.org/10.1111/jipb.70029

[38] Park CJ, Shin R. Calcium channels and transporters: Roles in response to biotic and abiotic stresses. Frontiers in Plant Science. 2022; 13: 964059. https://doi.org/10.3389/fpls.2022.964059

[39] Kashem MA, Itoh K, Iwabuchi S, Hori H, Mitsui T. Possible involvement of phosphoinositide-Ca2+ signaling in the regulation of alpha-amylase expression and germination of rice seed (Oryza sativa L.). Plant & Cell Physiology. 2000; 41: 399–407. https://doi.org/10.1093/pcp/41.4.399

[40] Li L, Wang F, Yan P, Jing W, Zhang C, Kudla J, et al. A phosphoinositide-specific phospholipase C pathway elicits stress-induced Ca^{2+} signals and confers salt tolerance to rice. The New Phytologist. 2017; 214: 1172–1187. https://doi.org/10.1111/nph.14426

[41] Zhang J, Ru X, You W, Xu F, Wu Z, Jin P, et al. Phosphatidylinositol-specific phospholipase C-associated phospholipid metabolism mediates DcGLRs channel to promote calcium influx under $CaCl_2$ treatment in shredded carrots during storage. International Journal of Biological Macromolecules. 2024; 270: 132517. https://doi.org/10.1016/j.ijbiomac.2024.132517

[42] Kiselev K, Dubrovina A. The role of calcium-dependent protein kinase (CDPK) genes in plant stress resistance and secondary metabolism regulation. Plant Growth Regulation. 2025; 105: 535–552. https://doi.org/10.1007/s10725-025-01295-6

[43] Liese A, Eichstädt B, Lederer S, Schulz P, Oehlschläger J, Matschi S, et al. Imaging of plant calcium-sensor kinase conformation monitors real time calcium-dependent decoding in planta. The Plant Cell. 2024; 36: 276–297. https://doi.org/10.1093/plcell/koad196

[44] Silamparasan D, Chang IF, Jinn TL. Calcium-dependent protein kinase CDPK16 phosphorylates serine-856 of glutamate receptor-like GLR3.6 protein leading to salt-responsive root growth in Arabidopsis. Frontiers in Plant Science. 2023; 14: 1093472. https://doi.org/10.3389/fpls.2023.1093472

[45] Fang X, Liu B, Kong H, Zeng J, Feng Y, Xiao C, et al. Two calcium sensor-activated kinases function in root hair growth. Plant Physiology. 2024; 196: 1534–1545. https://doi.org/10.1093/plphys/kiae365

[46] Liu S, Zhao L, Cheng M, Sun J, Ji X, Ullah A, et al. Calmodulins and calmodulin-like proteins-mediated plant organellar calcium signaling networks under abiotic stress. The Crop Journal. 2024; 12: 1321–1332. https://doi.org/10.1016/j.cj.2024.09.006

[47] Zeng H, Zhu Q, Yuan P, Yan Y, Yi K, Du L. Calmodulin and calmodulin-like protein-mediated plant responses to biotic stresses. Plant, Cell & Environment. 2023; 46: 3680–3703. https://doi.org/10.1111/pce.14686

[48] Wang C, Luan S. Calcium homeostasis and signaling in plant immunity. Current Opinion in Plant Biology. 2024; 77: 102485. https://doi.org/10.1016/j.pbi.2023.102485

[49] Wang W, Cheng HY, Zhou JM. New insight into Ca^{2+} -permeable channel in plant immunity. Journal of Integrative Plant Biology. 2024; 66: 623–631. https://doi.org/10.1111/jipb.13613